Acústica 2020
XI Congreso Ibérico de Acústica
51º Congreso Español de Acústica
TECNIACÚSTICA 2020

PREDICTION OF PILE DRIVING INDUCED VIBRATIONS BASED ON TIME DOMAIN FINITE ELEMENT SIMULATION

Tales Vieira Sofiste[1], Luís Godinho[1], Pedro Alves Costa[2], Delfim Soares[3]

[1]University of Coimbra, ISISE, Department of Civil Engineering
{tales.sofiste@uc.pt, lgodinho@dec.uc.pt}
[2]University of Porto, CONSTRUCT, Department of Civil Engineering
{pacosta@fe.up.pt}
[3]Federal University of Juiz de Fora, Department of Structural Engineering
{delfim.soares@ufjf.edu.br}

Resumo
Cravação de estacas é uma das técnicas mais antigas utilizada na construção de fundações profundas e ainda amplamente empregada nas construções modernas. Apesar de suas inúmeras vantagens técnicas, este método induz a propagação de vibrações significativas no terreno. Estas vibrações interagem com estruturas vizinhas e podem causar perturbação para os utilizadores ou até danos estruturais, em casos mais extremos. No presente trabalho, um modelo numérico para a previsão de vibrações induzidas pela cravação de estacas por vibração é apresentado. Nesta abordagem, o método dos elementos finitos no domínio do tempo é utilizado, considerando um eficiente método semiexplícito/explícito de marcha no tempo. A formulação numérica é apresentada e posteriormente é realizado um exemplo de aplicação. Os resultados obtidos são comparados com estudos disponíveis na literatura e demonstram o bom desempenho do método proposto.

Palavras-chave: cravação de estacas, vibrações, método dos elementos finitos, simulação no domínio do tempo.

Abstract
Pile driving operation is one of the oldest methods for constructing foundations and it is still widely employed in modern constructions. Besides its numerous technical advantages, this method induces ground-borne vibrations. These vibrations interfere with nearby structures and may cause disturbance to building users or even structural damage, in extreme cases. In this work, an effective numerical model for the prediction of vibrations induced by vibratory pile driving is presented. In this approach, the finite element method is employed in the time domain considering an efficient semi-explicit/explicit time marching procedure. The numerical formulation is presented and an application example is carried out. The obtained results are compared with previous studies and demonstrate the good performance of the proposed model.

Keywords: pile driving, vibrations, finite element method, time domain simulation.

PACS no. 43.40.At

1 Introduction

Numerical methods have numerous applications for dealing with complex problems in various branches of science and engineering. Several numerical approaches are available in the literature for the prediction of ground-borne vibrations induced by railway traffic [1,2], road traffic [3,4] and pile driving [5,6,7]. In the present work, a numerical model based on time domain finite element method (FEM) is developed for the study of vibratory pile driving. This traditional foundation technique presents various advantages and is still widely used in modern constructions, despite its environmental disturbance. Concerning its negative aspects, noise and air pollution are relatively easy to overcome with adequate isolation measures [8]. On the other hand, ground-borne vibrations are difficult to predict and, in most cases, considerably expensive to mitigate. In the vast majority of practical engineering applications, the peak particle velocity (PPV) is still estimated according to simplified empirical energy-based methods [9]. However, empirical models usually disregard fundamental features of the pile driving operation and of the response of the system [8]. Thus, a numerical model for the prediction of ground-borne vibrations induced by vibratory pile driving is implemented in this work. In order to do so, the finite element method in time domain is employed, considering an innovative and entirely automatized time marching technique [10]. A case study is carried out and the computed results are compared with previous numerical studies and field measurements available in the literature.

2 Governing equations and time marching procedure

The governing system of equations of a dynamic model, considering time domain FEM formulation, is given by [11]:

$$\mathbf{M}\ddot{\mathbf{U}}(t) + \mathbf{C}\dot{\mathbf{U}}(t) + \mathbf{K}\mathbf{U}(t) = \mathbf{F}(t) \tag{1}$$

where $\ddot{\mathbf{U}}(t)$, $\dot{\mathbf{U}}(t)$ and $\mathbf{U}(t)$ stand for acceleration, velocity and displacement vectors, respectively; $\mathbf{F}(t)$ stands for the applied force vector and $\mathbf{M}$, $\mathbf{C}$ and $\mathbf{K}$ stand for mass, damping and stiffness matrices, respectively. The initial conditions of this system are: $\mathbf{U}(0) = \mathbf{U}^0$ and $\dot{\mathbf{U}}(0) = \dot{\mathbf{U}}^0$ (where $\mathbf{U}^0$ and $\dot{\mathbf{U}}^0$stand for the initial displacement and initial velocity vector, respectively). The equation of motion (Equation 1) is solved employing a semi-explicit/explicit time marching proposed by Soares [10]. Once linear analysis is the focus of the present work, a simplified approach of this time integration scheme is presented here. In this novel technique, the standard Central Difference Method (CDM), a conditionally stable, second order accurate, explicit method, is employed for the approximations of the time derivative of the displacements field, which are defined as:

$$\ddot{\mathbf{U}}^n = \frac{1}{\Delta t^2}(\mathbf{U}^{n+1} - 2\mathbf{U}^n + \mathbf{U}^{n-1}) \tag{2}$$

$$\dot{\mathbf{U}}^n = \frac{1}{2\Delta t}(\mathbf{U}^{n+1} - \mathbf{U}^{n-1}) \tag{3}$$

where n indicates the time step of the variable and Δt stand for the time step of the analysis. The adopted time integration scheme is locally defined (the subscript "*e*" indicates that the variable is local), based on the following recursive relation:

$$\left(\bar{\mathbf{M}}_e + \frac{1}{2}\Delta t\mathbf{C}_e\right)\mathbf{U}_e^{n+1} = \Delta t^2(\mathbf{F}_e^n - \mathbf{K}_e\mathbf{U}_e^n) + \bar{\mathbf{M}}_e(2\mathbf{U}_e^n - \mathbf{U}_e^{n-1}) + \frac{1}{2}\Delta t\mathbf{C}_e\mathbf{U}_e^{n-1} \tag{4}$$

which reproduces the standard CDM when $\bar{\mathbf{M}}_e = \mathbf{M}_e$ is adopted. The modified local mass matrix $\bar{\mathbf{M}}_e$ is given by:

$$\bar{\mathbf{M}}_e = \mathbf{M}_e + \Delta t^2 a_e \mathbf{K}_e \tag{5}$$

where a_e is a local parameter, defined in order to ensure the stability of the method. As it is well stablished, the CDM is conditionally stable and presents a critical sampling frequency $\Omega_c = 2$. The idea of the adopted time marching procedure is to evaluate the maximum sampling frequency of each element and, if they are greater than 2, to compute a proper value for a_e in order to assure the stability of the element. Therefore, the parameter a_e is automatically computed as follows:

$$\text{if } \Omega_e^{max} \leq 2,\ a_e = 0 \tag{6}$$

$$\text{if } \Omega_e^{max} > 2,\ a_e = \frac{1}{4}\tanh\left(\frac{1}{4}\Omega_e^{max}\right) \tag{7}$$

where Ω_e^{max} stand for the maximum sampling frequency of the element. Thus, the standard explicit CDM is reproduced whenever $\Omega_e^{max} \leq 2$ (stable element) and an effective implicit method arises otherwise (stabilized element). The variable Ω_e^{max} is calculated as follows:

$$\Omega_e^{max} = \omega_e^{max} \Delta t \tag{8}$$

where ω_e stands for the maximum natural frequency of the element, computed as the square root of the maximum eigenvalue of the locally defined generalized eigenvalue problem [12], given by:

$$\mathbf{K}_e \phi_e = \omega_e^2 \mathbf{M}_e \phi_e \tag{9}$$

Hence, this time integration scheme is simple to implement and quite efficient, since explicit and implicit subdomains are automatically generated according to the geometrical and physical properties of the discretized model. In addition, it is entirely automatized and requires no decision or expertise from the user (which must only define the time step of the analysis).

3 Numerical modelling

3.1 Model dimensions and properties

Three penetration scenarios are studied in this work ($h_1 = 2$ [m], $h_2 = 5$ [m] and $h_3 = 10$ [m]), since the penetration depth plays a significant role in the propagation pattern. The finite element method, considering an axisymmetric formulation is implemented with triangular quadratic elements (6 nodes). In addition, a lumped mass matrix is considered, which is a requirement of explicit time marching procedures. The mass diagonalization is computed employing the diagonal scaling procedure proposed by Zienkiewicz et al. [13]. The adopted dimensions of the numerical model are $H = 20$ [m] (depth) and $L = 30$ [m] (length). A sketch of the model considering the third penetration scenario ($h_3 = 10$ [m]) is depicted in Figure 1.

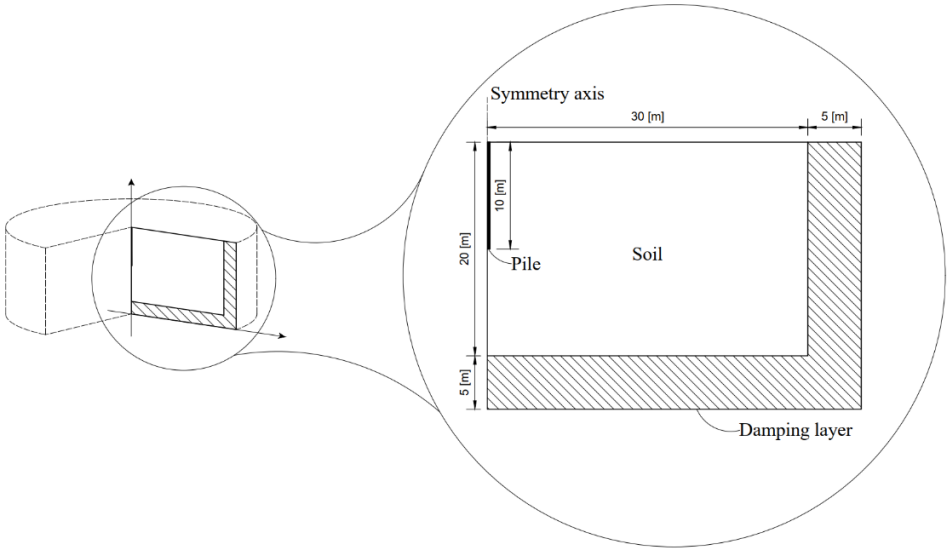

Figure 1 – Sketch of the numerical model for $h_3 = 10$ [m].

The damping ratio of the soil is considered as $\xi = 2.5$ % (the numerical approach of the physical damping matrix is presented in Section 3.2). As one may observe, a damping layer ($L_{damp} = 5$ [m]) is also considered, which is computed with a linear increasing damping factor from $\xi = 2.5$ % up to $\xi = 100$ % in the end of the domain. This damping layer is implemented to avoid spurious wave reflections on the boundaries of the domain and simulate an infinite medium. A concrete pile is considered with $L_p = 10$ [m] (pile length) and $d_p = 0.5$ [m] (pile diameter). The soil and pile physical properties (Table 1) are the same as the ones employed by Masoumi et al. [6], in order to evenly compare the obtained results.

Table 1 – Soil and pile properties.

Property	Soil	Pile
Young modulus	$E_s = 80$ [MPa]	$E_p = 40$ [GPa]
Poisson ratio	$\nu_s = 0.40$ [−]	$\nu_p = 0.25$ [−]
Mass density	$\rho_s = 2000$ [kg/m^3]	$\rho_p = 2500$ [kg/m^3]

The finite element mesh is generated in *Gmsh* [14] with approximately 72000 nodes and 36000 elements (the number of nodes and elements varies accordingly to the penetration depth considered). The critical time step for the three studied scenarios is $\Delta t_c = 7.1899 \times 10^{-6}$ [s] (conservatively evaluated considering the critical values of each element) and the adopted time step is $\Delta t = 2 \times 10^{-4}$ [s]. Thus, following the formulation presented in Section 2, explicit and implicit subdomains are automatically generated accordingly to the physical and geometrical properties of each element. The number of explicit and implicit elements for each penetration depth is shown in Table 2. In addition, the domain decomposition for the penetration depth $h_3 = 10$ [m] is depicted in Figure 2.

Table 2 – Properties of the FEM meshes adopted.

Penetration depth	Nodes	Elements	Explicit elements	Implicit elements
$h_1 = 2$ [m]	72412	35933	25762 (71.69%)	10171 (28.31%)
$h_2 = 5$ [m]	72339	35910	25750 (71.71%)	10160 (28.29%)
$h_3 = 10$ [m]	72192	35859	25726 (71.74%)	10133 (28.26%)

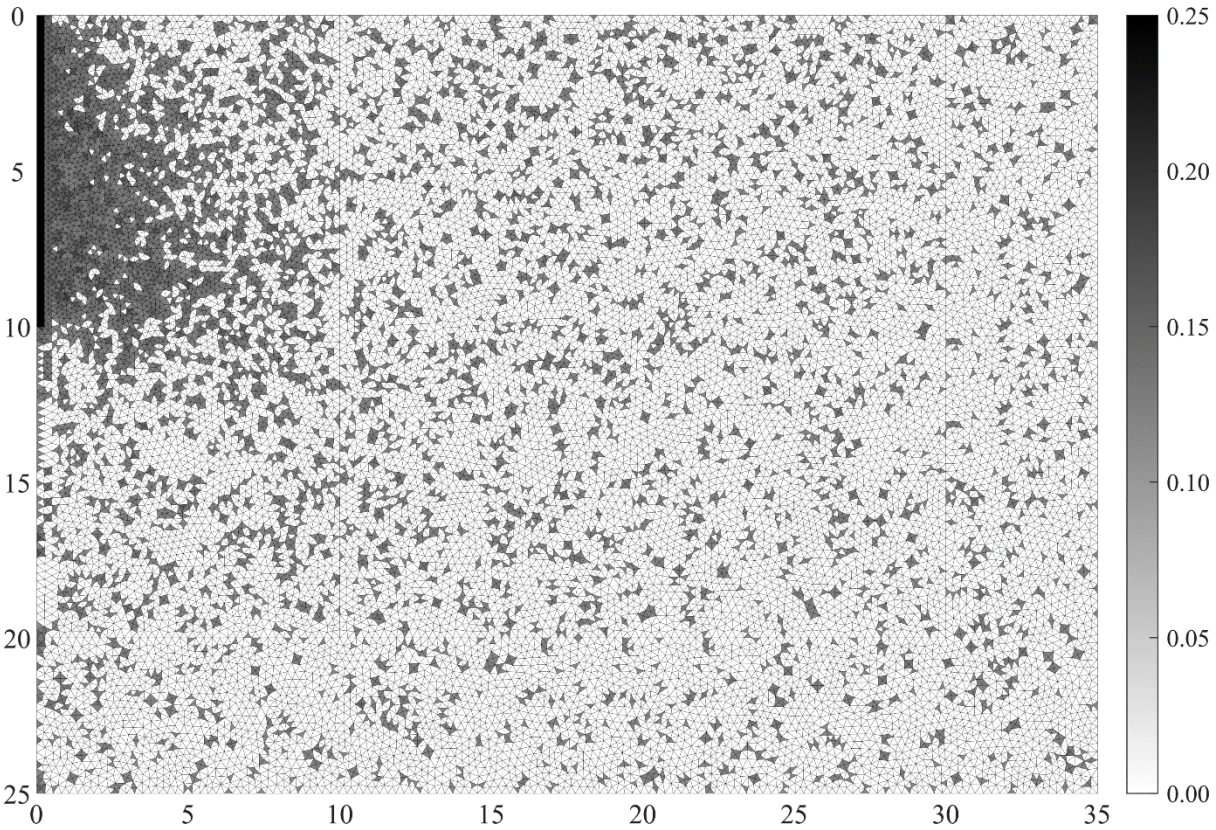

Figure 2 – Domain decomposition for $h_3 = 10$ [m]. White elements correspond to explicit elements ($a_e = 0$) and grey/black elements correspond to implicit elements ($a_e > 0$).

3.2 Physical damping approach

As previously discussed, the lumped mass matrix is obtained by employing the diagonal scaling procedure [13]. In addition, the time marching scheme adopted in this work presents explicit and implicit subdomains in the same analysis. In order to fully explore the advantages of the method, a diagonal damping matrix must be employed in the explicit subdomain. Thus, a mass proportional damping matrix is considered for the model, which is evaluated as:

$$\mathbf{C}_e = \gamma \mathbf{M}_e \tag{10}$$

where γ is defined as:

$$\gamma = 2\xi\omega_k \tag{11}$$

where ω_k stands for the control frequency (in [rad/s]), assumed here equal to the loading frequency (see Section 4.1):

$$\omega_k = 125.66\ [\text{rad/s}] = 20\ [\text{Hz}] \tag{12}$$

Thus, the parameter γ is given by:

$$\gamma = 6.2832 \tag{13}$$

The actual damping ratio applied in the model versus frequency (in [Hz]) is depicted in Figure 3. It is important to highlight that, in the adopted damping approach, the physical damping varies according to the frequency. The idea here is to assure the adopted damping ratio ($\xi = 2.5\%$) for the loading frequency (20 [Hz]).

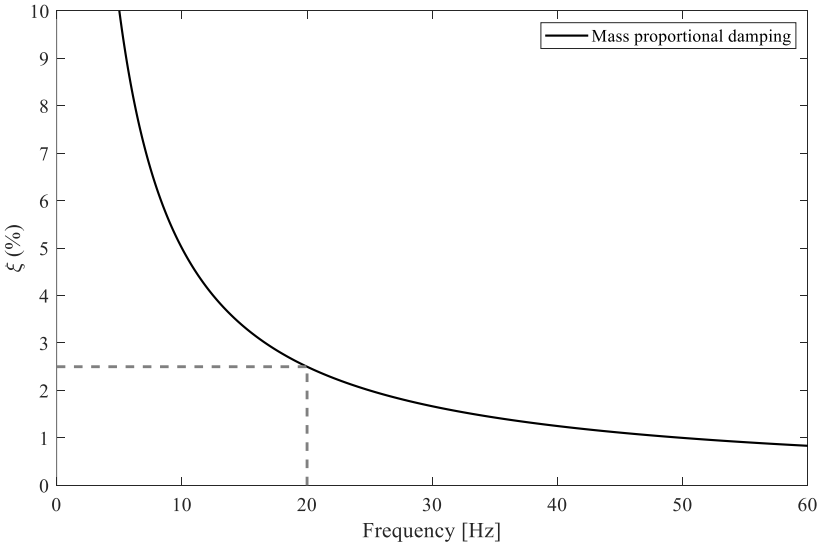

Figure 3 – Physical damping of the model.

4 Case study

4.1 Vibratory driving force

A case study is presented in this section, with a numerical model developed according to the previously described methodologies. The same properties and assumptions adopted by Masoumi et al. [6] are considered here. A sinusoidal force is applied at the center of the pile head, in order to simulated an ICE 44-30V hydraulic vibratory hammer [6]. This force is computed as:

$$F(t) = me\ (2\pi f)^2 \sin(2\pi f\ t) \tag{14}$$

where $f = 20$ [Hz] is the operation frequency of the equipament and $me = 50.7$ [kg m] is the excentric moment. Thus, the maximum applied dynamic force is $F_{max} = 800$ [kN]. It should be stressed that this load is added to the static load imposed by the weight of the driving device.

4.2 Results and discussion

In this numerical application, ground vibrations due to vibratory pile driving are studied for three penetration depths ($h_1 = 2$ [m], $h_2 = 5$ [m] and $h_3 = 10$ [m]). Figure 4 shows the norm of the particle velocity for the considered scenarios. As one may observe, the damping layer is not depicted in the snapshots, but it is working properly, since no spurious reflections are occurring in the boundary of the

domain. It also may be observed that a larger amount of energy is presented for the lowest penetration depth (Figure 4(a)) when compare with the deeper scenario (Figure 4(c)). This complex behavior occurs mainly because two wave fronts are generated during the pile driving operation: from the pile shaft and from the pile toe. The interaction between these waves and the ground surface induces the formation of Rayleigh waves. In this sense, lower penetration depths lead to a smaller distance between the pile toe and the ground surface, which lead to higher amount of energy that reach the surface and that is converted to Rayleigh waves (Figure 4(a)). The opposite behavior is observed for deeper scenarios (Figure 4(c)). In addition, the implemented model correctly simulated the separation between the surface waves (located at the ground surface) and the body waves (located in the depths of the ground), which travel in slightly different velocities.

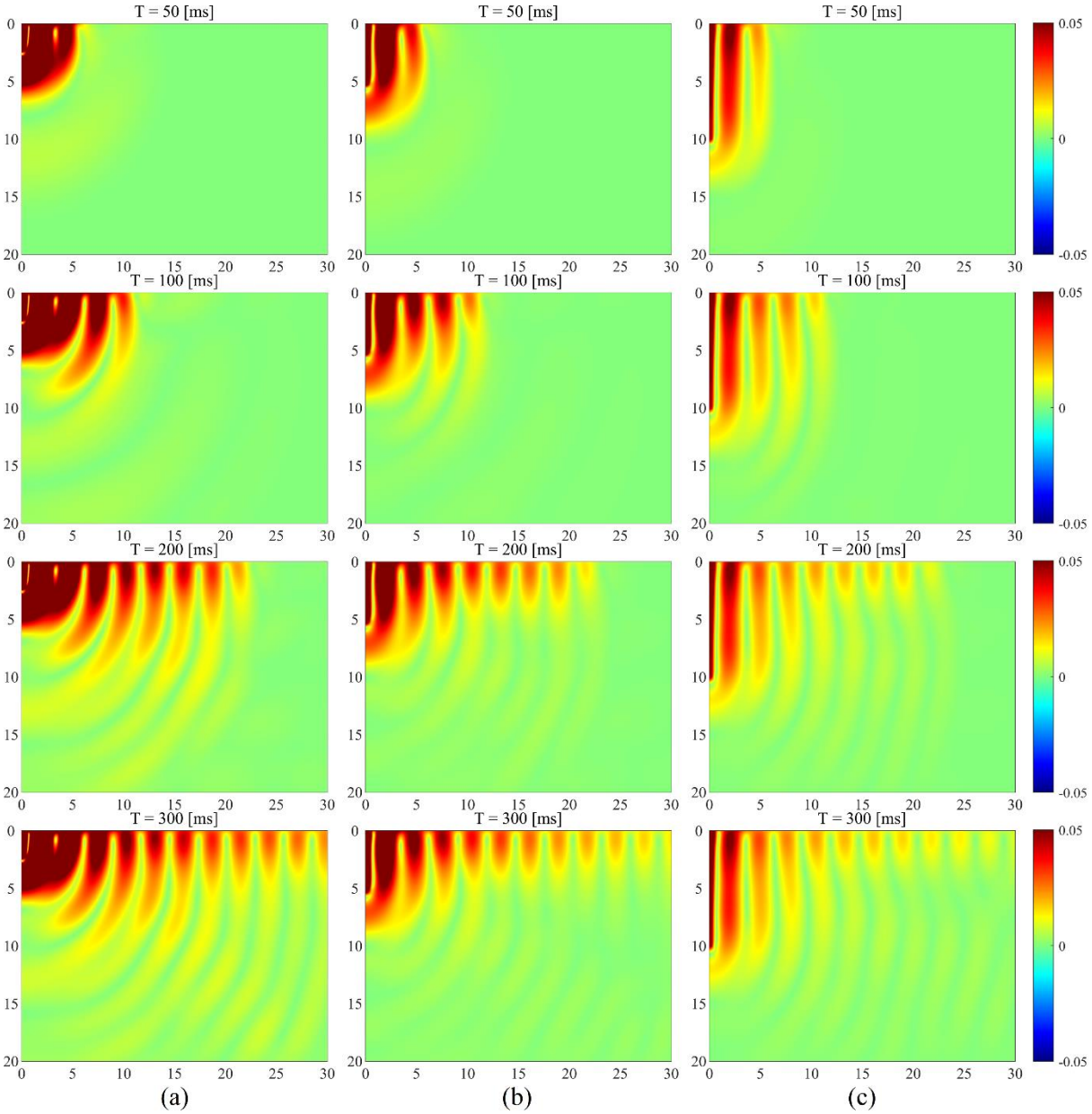

Figure 4 – Snapshots of the norm of the particle velocity: (a) $h_1 = 2$ [m], (b) $h_2 = 5$ [m] and (c) $h_3 = 10$ [m].

The particle trajectories for three ground points located at $r = 0.5$ [m], $r = 5$ [m] and $r = 10$ [m] for the three penetration scenarios studied are presented in Figure 5. The different types of waves generated during the vibratory pile driving are correctly simulated by the model. For the point located near the vicinity of the pile ($r = 0.5$ [m]), a domination of vertical displacement is observed, which demonstrates the presence of SV-waves. For the points located far away from the pile ($r = 5$ [m] and $r = 10$ [m]), the particle displacement presents an elliptical pattern, typical of Rayleigh waves. Thus, body waves are mostly attenuated in the far field and the ground vibrations are mainly dominated by surface waves.

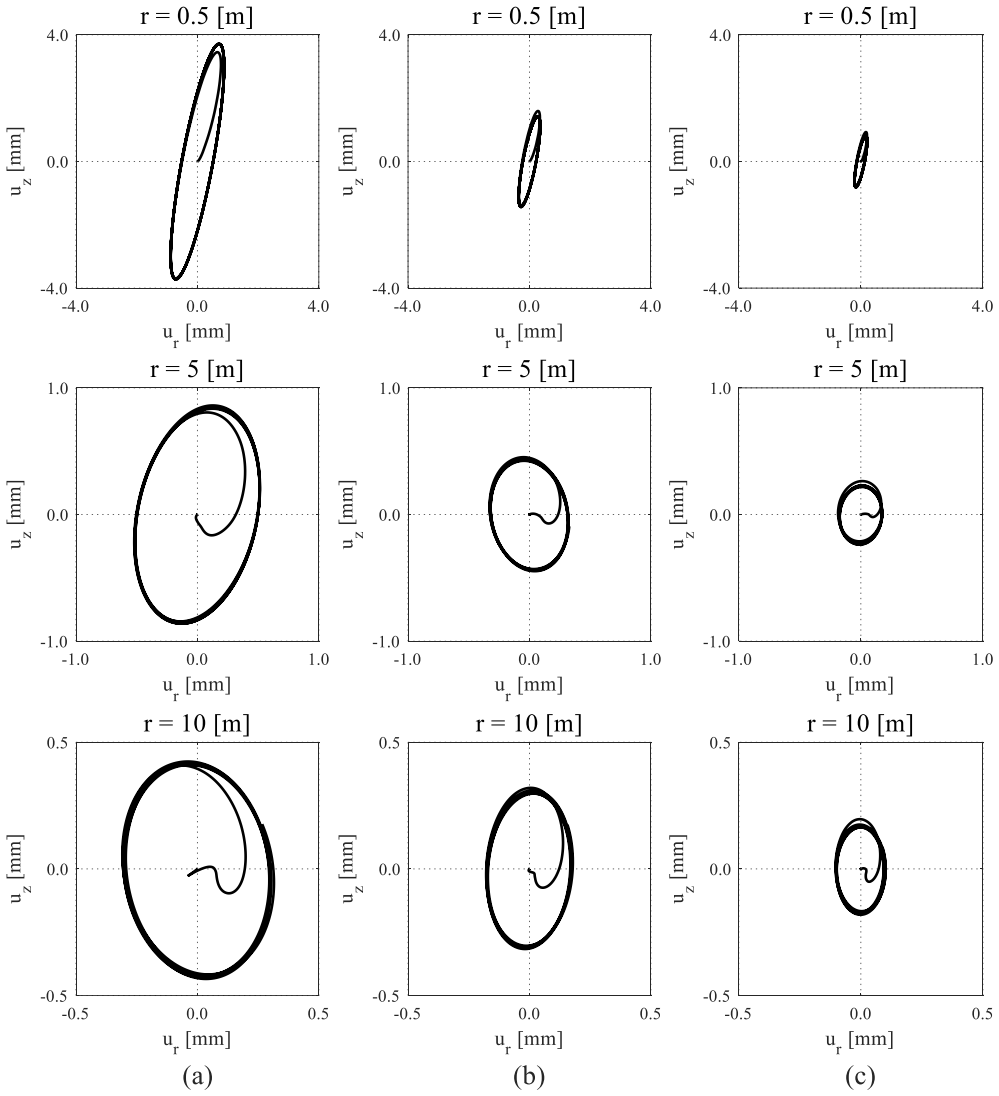

Figure 5 – Particle trajectories of ground points at radial distance $r = 0.5$ [m], $r = 5$ [m] and $r = 10$ [m] for three penetration depths: (a) $h_1 = 2$ [m], (b) $h_2 = 5$ [m] and (c) $h_3 = 10$ [m].

Figure 6 shows the variation of the PPV versus the depth at $r = 0.5$ [m] and $r = 10$ [m]. Since the strain measure is proportional to the peak particle velocity, this figure may be interpreted as the shear deformation of the soil [9]. For smaller penetration depth, the PPV is larger and decreases quickly over ground depth. On the other hand, for deeper penetration scenarios the PPV has a smaller magnitude but the variation along the pile shaft is smooth. This pattern is consistent with the previous results (Figure

4), since the energy is mostly located at the surface for smaller penetration depths. In Figure 7, the peak particle velocity versus the radial distance is presented. It is important to highlight that the case study presented by Masoumi et al. [6] is reproduced here, in order to compare the computed results. The slope of the vibration attenuation is quite similar to the previous numerical approach. However, a conservative prediction is obtained considering the field measurement presented, since plastic deformations are not accounted in these numerical models.

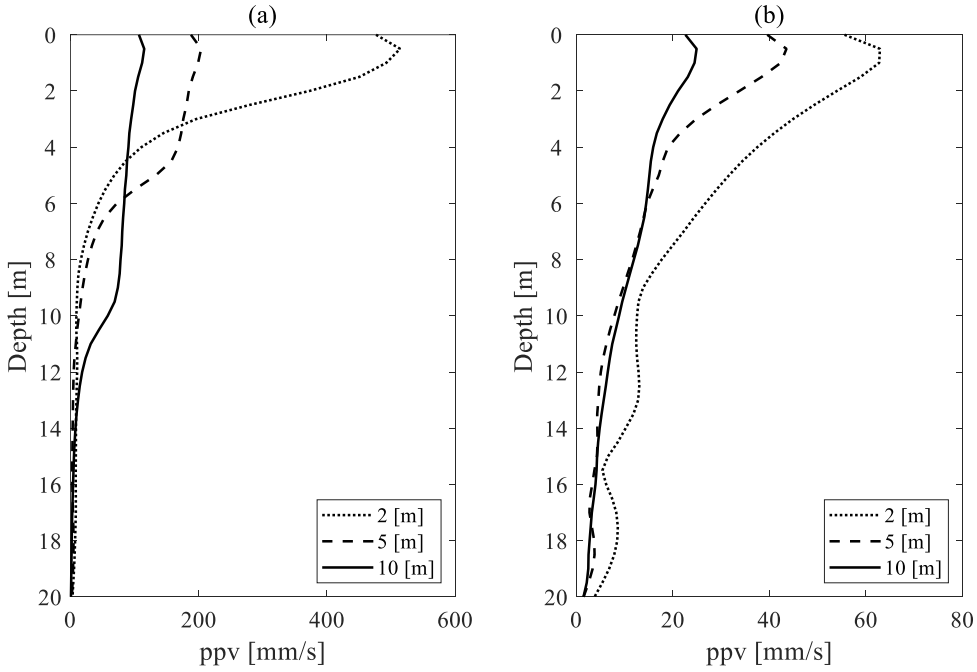

Figure 6 – PPV versus depth for the radial distance (a) $r = 0.5$ [m] and (b) $r = 10$ [m].

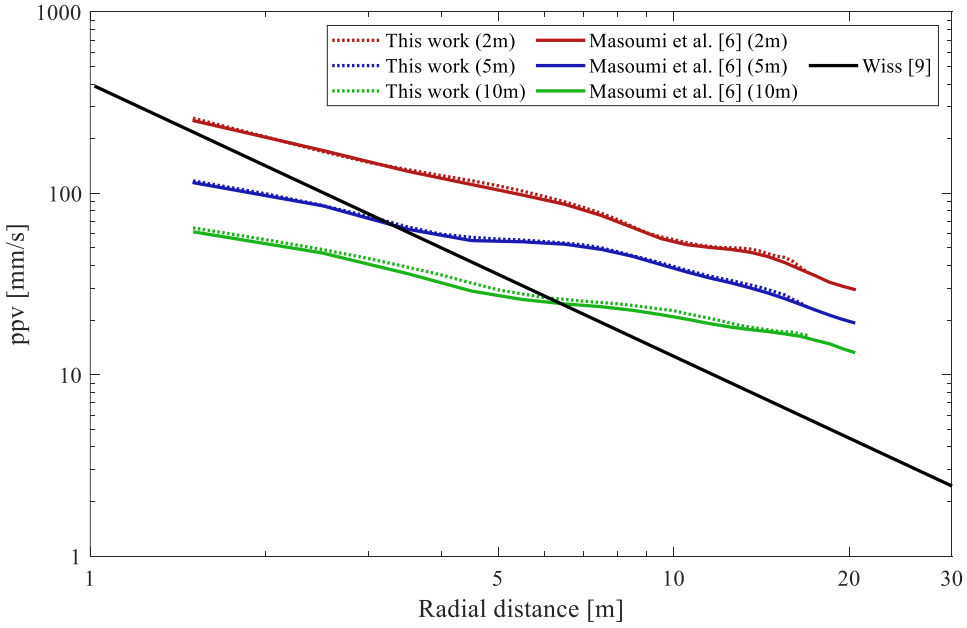

Figure 7 – PPV versus radial distance for several penetration depths.

5 Conclusions

An efficient time domain finite element model is developed for the prediction of ground-borne vibrations due to vibratory pile driving. An axisymmetric formulation is considered, which presents excellent results with a considerably smaller computational cost. Furthermore, the effective time marching procedure adopted also allowed to diminish the computational costs, since implicit (and more expensive) subdomains were automatically generated only when necessary, according to the stability of the model. A case study was carried out and the same properties available in the literature were employed, in order to obtain a consistent comparison. The computed results presented good agreement with previous numerical and empirical studies, which demonstrate the applicability of the proposed numerical model. In addition, the body waves and surface waves generated during the vibratory pile driving operation were correctly simulated. The linear constitutive model is a conservative approach for the behavior of the soil. In fact, large strains occur in the vicinity of the pile, which is not compatible with linear analysis. Therefore, the proposed methodology will be extended to nonlinear behavior in future works.

Acknowledgements

This work was financed by: project "VIPIB: Vibrations induced by pile driving in buildings: an integrated methodology for prediction and mitigation" – POCI-01-0145-FEDER-0029634, funded by FEDER funds through COMPETE2020 – Programa Operacional Competitividade e Internacionalização (POCI) and by national funds (PIDDAC) through FCT/MCTES; by FCT – Fundação para a Ciência e a Tecnologia, I.P., within the scope of the research unit "Institute for sustainability and innovation in structural engineering - ISISE" (UIDP/04029/2020); by the Regional Operational Programme CENTRO2020 within the scope of project CENTRO-01-0145-FEDER-000006 (SUSpENsE); and by: Base Funding (UIDB/04708/2020) and Programmatic Funding (UIDP/04708/2020) of the CONSTRUCT - Instituto de I&D em Estruturas e Construções - funded by national funds through the FCT/MCTES (PIDDAC). The financial support by CNPq (Conselho Nacional de Desenvolvimento Científico e Tecnológico) and FAPEMIG (Fundação de Amparo à Pesquisa do Estado de Minas Gerais) is also greatly acknowledged.

FCT Fundação para a Ciência e a Tecnologia

MINISTÉRIO DA CIÊNCIA, TECNOLOGIA E ENSINO SUPERIOR

References

[1] Lopes, P.; Alves Costa, P.; Ferraz, M.; Calçada, R.; Silva Cardoso, A. Numerical modeling of vibrations induced by railway traffic in tunnels: From the source to the nearby buildings. *Soil Dynamics and Earthquake Engineering*, Vol. 61-62, 2014, pp. 269-285.

[2] Galvín, P.; François, S.; Schevenels, M; Bongini, E.; Degrande, G.; Lombaert, G. A 2.5D FE-BE model for the prediction of railway induced vibrations. *Soil Dynamics and Earthquake Engineering*, Vol. 30(12), 2010, pp. 1500-1512.

[3] Lombaert, G.; Degrande, G.; Cloteau, D. Numerical modelling of free field traffic-induced vibrations. *Soil Dynamics and Earthquake Engineering*, Vol.19(7), 2000, pp. 473-488.

[4] Ju, S-H.; finite element investigation of traffic induced vibrations. *Journal of Sound and Vibration*, Vol. 321(3), 2009, pp. 837-853.

[5] Mabsout, M.E.; Tassoulas, J.L. A finite element model for the simulation of pile driving. *International Journal for Numerical Methods in Engineering*, Vol. 37(2), 1994, pp. 257-278.

[6] Masoumi, H.R.; Degrande, G.; Lombaert, G. Prediction of free field vibrations due to pile driving using a dynamic soil-structure interaction formulation. *Soil Dynamics and Earthquake Engineering*, Vol. 27(2), 2007, pp. 126-143.

[7] Masoumi, H.R.; François, S.; Degrande, G. A non-linear coupled finite element–boundary element model for the prediction of vibrations due to vibratory and impact pile driving. *International Journal for Numerical and Analytical Methods in Geomechanics*, Vol. 33(2), 2009, pp. 245-274.

[8] Massarsch, K.R.; Fellenius, B.H. Ground Vibrations Induced by Impact Pile Driving. *Sixth International Conference on Case Histories in Geotechnical Engineering*, Arlington, VA, August 11-16, 2018, pp. 1-38.

[9] Wiss, J.F. Construction vibrations: state-of-the-art. *Journal of Geotechnical and Geoenvironmental Engineering*, Vol. 107, 1981, pp. 167-181.

[10] Soares Jr., D. An adaptive semi-explicit/explicit time marching technique for nonlinear dynamics. *Computer Methods in Applied Mechanics and Engineering*, Vol. 354, 2019, pp.637-662.

[11] Clough, R.W.; Penzien, J. *Dynamics of structures*, Computers & Structures, Inc, Berkeley - CA, 1995.

[12] Bathe, K.J. *Finite Element Procedures (2nd Edition)*, Klaus-Jürgen Bathe, Watertown - MA, 2014.

[13] Zienkiewicz, O.C.; Taylor, R.L.; Zhu, J.Z. *The Finite Element Method: Its Basis and Fundamentals (6th Edition)*, Butterworth-Heinemann, Oxford, 2005.

[14] Geuzaine, C.; Remacle, J.F. Gmsh: A 3-D finite element mesh generator with built-in pre-and post-processing facilities. *International Journal for Numerical Methods in Engineering*, Vol. 79(11), 2009, pp. 1309-1331.